Electronic Supplementary Material (ESI) for Physical Chemistry Chemical Physics.

Supporting Information:

Kinetics of the reaction of OH with methyl nitrate (232–343 K)

Christin Fernholz[a], Fabienne Baumann[a], Jos Lelieveld[a] and John N. Crowley*[a]

[a]*Atmospheric Chemistry Department, Max Planck Institute for Chemistry, 55128 Mainz, Germany.*

1 Assessment of impurities in the CH_3ONO_2 sample

The concentrations of potential impurities HNO_3 and CH_3OH were assessed using FTIR spectroscopy. The spectrum of CH_3ONO_2 along with vibrational assignments is displayed below. The insets show absorption features of HNO_3 and CH_3OH from reference spectra obtained using the same apparatus. The commercial methanol sample was purified by freeze-pump-thaw cycles and HNO_3 was synthesised by mixing potassium nitrate and 98 % sulphuric acid. As described in the manuscript, neither HNO_3 nor CH_3OH were detected, enabling upper limits to their concentrations to be derived.

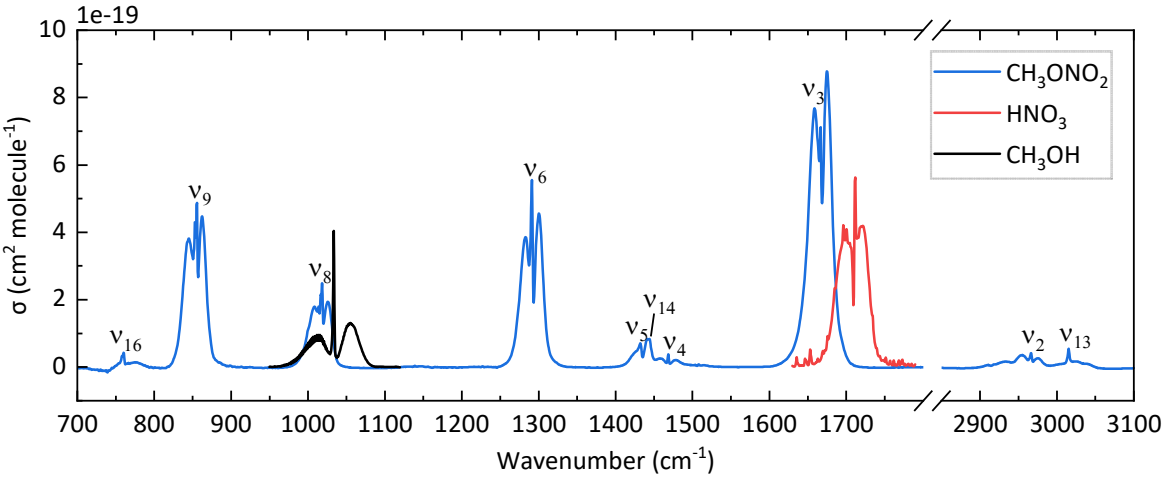

Figure S1: Gas-phase FTIR spectrum of methyl nitrate (blue) in the range 700-3100 cm^{-1}. The vibrational frequencies are assigned according to the literature[4]. Absorption features of HNO_3 (1.27×10^{15} molecule cm^{-3}, scaled by factor 0.5, red) and CH_3OH (1.14×10^{15} molecule cm^{-3}, scaled by factor 0.025, black), respectively. The concentrations of CH_3OH and HNO_3 were derived from simultaneously measured optical extinction at 185 nm.

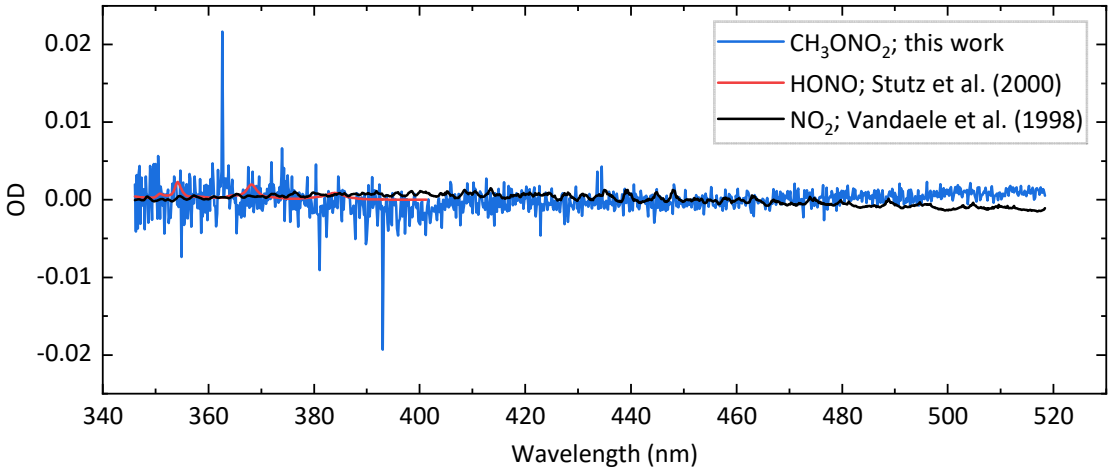

Figure S2: Optical density (blue) of a flowing sample of CH_3ONO_2 (1.86×10^{16} molecule cm^{-3}) in regions where HONO and NO_2 absorb. The red and black lines are calculated optical densities, based on measurements by Stutz et al.[3] and Vandaele et al.[5], for HONO (5×10^{12} molecule cm^{-3}) and NO_2 (5×10^{12} molecule cm^{-3}).

2 Use of CH_3ONO_2 photolysis to generate OH

As described in the manuscript, the 248 nm photolysis of CH_3ONO_2 to generate OH results in bi-exponential OH profiles (Figure 5), the analysis of which does not lead to the same rate coefficient k_4 as derived from experiments in which HONO was photolyzed at 351 nm to generate OH. This behaviour contradicts the results of Talukdar et al.[7], who were able to derive a reasonably accurate rate coefficient with this method. We identify two reasons why, in our study, the photolysis of CH_3ONO_2 does not lead to the correct value of k_4.

1) Co-detection of OH and CH_3O

A potential explanation for a bias in k_4 is the undesired co-detection of CH_3O as well as OH. As CH_3O is formed directly at high yield whereas OH is formed after conversion of an H-atom (itself formed at low yield) to OH via reaction with CH_3ONO_2, CH_3O is expected to be present at a much larger concentration than OH. Figure S3 (green trace) shows the LIF-excitation spectra obtained at discrete steps when CH_3ONO_2 is photolyzed at 248 nm. Clearly, the excitation spectrum obtained is a composite of OH and CH_3O, which will preclude the determination of k_4 based on the assumption that the LIF signal obtained with excitation at 282 nm is due to OH only.

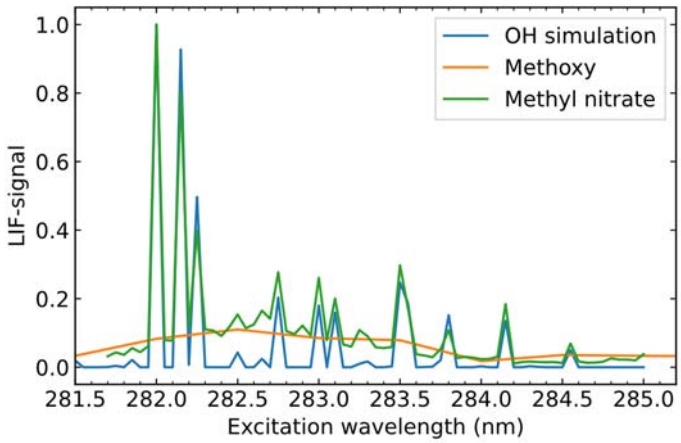

Figure S3: Green-trace: The fluorescence excitation spectrum (measured at discrete steps of 0.05 nm) observed when photolyzing methyl nitrate at 248 nm. Blue-trace: The simulated fluorescence excitation spectrum of OH (LIFBASE 2.1[2]) with a resolution of 0.125 Å plotted at the same discrete steps. Orange-trace: fluorescence excitation spectrum of CH_3O with a step size of 0.5 nm, obtained by photolyzing CH_3ONO at 248 nm.

2) Reaction of OH with CH_3O and NO_2 and further secondary chemistry

The CH_3O and NO_2 photo-fragments formed when CH_3ONO_2 is photolyzed at 248 nm is expected to result in a dependence of the OH decay constant on the energy of the photolysis laser. This was explored using numerical simulation Facsimile[1] of an assumed reaction scheme (see below). Figure S4 shows that taking into account the side reactions of OH with CH_3O, NO_2 and CH_2O results in a deviation (a bias to larger values) compared to the expected rate constant at various photolysis energies (up to 10mJ / pulse).

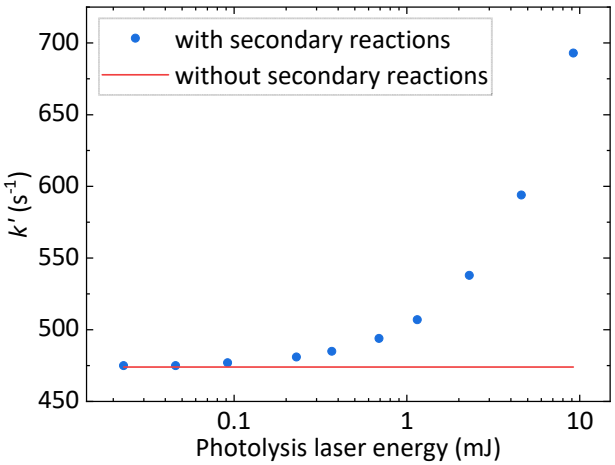

Figure S4: First-order decay coefficients *k*' plotted against photolysis laser energy. In blue, *k*' determined via numerical simulation[1], accounting for secondary reactions of OH with CH_3O, NO_2, and CH_2O. The reactions considered in the simulation are shown in Table S1. In red, OH decay constant, calculated from the CH_3ONO_2 concentration used in the simulation and the rate coefficient determined in this work (i.e. without secondary losses of OH).

Table S1: Reactions considered in the simulation. Rate coefficients correspond to 298 K and 100 Torr N_2.

Reaction	Rate coefficient	source
$H_2O_2 + h\nu \rightarrow OH + OH$	a	IUPAC[8]
$CH_3ONO_2 + h\nu \rightarrow CH_3O + NO_2$	a	Talukdar et al.[7]
$CH_3ONO_2 + h\nu \rightarrow H + CH_2O + NO_2$	a	Talukdar et al.[7]
$CH_3O + NO_2 + M \rightarrow CH_3ONO_2 + M$	b1	IUPAC[8]
$OH + CH_3ONO_2 \rightarrow H_2O + CH_2O + NO_2$	2.3e-13	This work
$OH + NO_2 + M \rightarrow HNO_3 + M$	b2	IUPAC[8]
$OH + H_2O_2 \rightarrow HO_2 + H_2O$	3.5e-12	IUPAC[8]
$OH + HO_2 \rightarrow H_2O + O_2$	1.1e-10	IUPAC[8]
$OH + CH_3O \rightarrow CH_2O + H_2O$	3.0e-11	Tsang and Hampson[9]
$OH + CH_2O \rightarrow H_2O + HCO$	8.5e-12	IUPAC[8]
$HO_2 + HO_2 \rightarrow H_2O_2 + O_2$	1.7e-13	IUPAC[8]
$H + CH_3ONO_2 \rightarrow OH + CH_3ONO$	1.6e-13	Talukdar et al.[7]
$H + NO_2 \rightarrow OH + NO$	1.3e-10	Burkholder et al.[10]
$HO_2 + CH_3O \rightarrow CH_3OH + O_2$	4.7e-11	Assaf et al.[11]
$NO + HO_2 \rightarrow OH + NO_2$	8.5e-12	IUPAC[8]

Listed rate coefficients are in cm^3 $molecule^{-1}$ s^{-1}. [a]Relative concentrations of OH, H and $CH_3O + NO_2$ were based on known cross-sections of H_2O_2 and CH_3ONO_2 and photolysis quantum yields at 248 nm. [b1, b2]Parameterisation with "Troe" expression using parameters listed by IUPAC to calculate the bimolecular rate coefficient $k(p,T)$. b1: $k_0 = 8.1 \times 10^{-29}$ $(T/300)^{-4.5}$ $[N_2]$ cm^3 $molecule^{-1}$ s^{-1}, $k_{inf} = 2.1 \times 10^{-11}$ cm^3 $molecule^{-1}$ s^{-1}, Fc = 0.44. b2: $k_0 = 3.2$ x 10-30 $(T/300)^{-4.5}$ $[N_2]$ cm^3 $molecule^{-1}$ s^{-1}, $k_{inf} = 3.0 \times 10^{-11}$ cm^3 $molecule^{-1}$ s^{-1}, Fc = 0.41. The "Troe" expression is:

$$k\ (p,T) = \frac{k_0\left(\frac{T}{300}\right)^{-m} M k_{\text{inf}}\left(\frac{T}{300}\right)^{-n}}{k_0\left(\frac{T}{300}\right)^{-m} M + k_{\text{inf}}\left(\frac{T}{300}\right)^{-n}} \log F$$

where

$$\log F = \frac{logF_c}{1 + \left[log\left(\frac{k_0\left(\frac{T}{300}\right)^{-m} M}{k_{\text{inf}}\left(\frac{T}{300}\right)^{-n}}\right)/N\right]^2}$$

3 Atmospheric lifetime of CH_3ONO_2

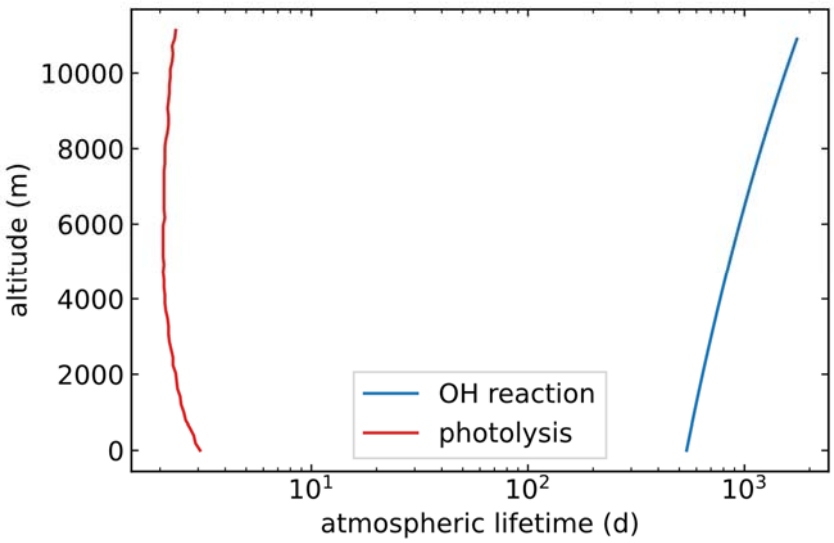

Figure S5: Altitude dependent atmospheric lifetimes (in days) of CH_3ONO_2 with respect to reaction with OH (blue, assuming a global mean concentration of 1×10^6, molecule cm^{-3} [6]). In red, the lifetime considering the photolysis, based on J-values from Talukdar et al.[7].

4 Calculation of uncertainties in the rate coefficient

The potential systematic bias of 5 % is an estimation based on the multiple determination of the absorption cross-section (Figure 1). To determine the absorption cross-section, a weighted linear fit if OD versus concentration is used and the resulting error is given by 2σ. For each point in Figure 1, the error for the optical density (ΔOD) is derived by averaging the measured OD and calculating the standard deviation of 2σ. The error in the x-direction, $\Delta(c \times l)$ is determinate by an error propagation of the following (estimated) errors $\Delta T = 1$ K, $\Delta p = 0$ Torr (better than 1‰) and $\Delta c_{\%} = 2$ % (c × 0.02). Following the equation for the error propagation:

$$\Delta(c \cdot l) = \pm 3.24 \times 10^{16} \times 298\text{K} \times \sqrt{\left(\frac{l\,p}{T}\Delta c_{\%}\right)^2 + \left(\frac{l\,c_{\%}}{T}\Delta p\right)^2 + \left(-\frac{l\,c_{\%}\,p}{T^2}\Delta T\right)^2 + \left(\frac{c_{\%}\,p}{T}\Delta l\right)^2}$$

The following fit equations are obtained from the respective weighted fit (orthogonal distance regression) for the two individual measurement series:

$y = [(1.69 \pm 0.07) \times 10^{-18}]x + (0.004 \pm 0.009)$ and $y = [(1.67 \pm 0.14) \times 10^{-18}]x + (-0.012 \pm 0.031)$,

where the slope corresponds to the absorption cross-section. The differences here result in a deviation of 1.2%. Both measurements together result in the following fit equation: $y = [(1.65 \pm 0.09) \times 10^{-18}]x + (0.002 \pm 0.015)$. By this measurement, we estimate the total error of the experiment to be 5%. Added to this is the statistical error from the various fits. A monoexponential fit (least squares) was used to determine *k*' and the standard deviation (2σ) was obtained with the value. These can be seen as error bars in Figure 3. Here, a weighted linear fit (least squares) was performed to determine *k*, which again outputs an error (2σ). This in turn can be seen as an error in the Arrhenius plot, where a weighted monoexponential fit (least squares) was also performed. As is often the case in such experiments, the scatter in the data is greater than the total uncertainty estimated as described above, which may indicate unidentified (and thus not assessable) sources of uncertainty.

References

1. A. R. Curtis and W. P. Sweetenham, *Facsimile, Atomic Energy Research Establishment, Report R-12805, 1987*, 1987.
2. J. Luque and D. R. Crosley, *LIFBASE (version 1.5)* http://www.sri.com/cem/lifbase, 1999.
3. J. Stutz, E. S. Kim, U. Platt, P. Bruno, C. Perrino and A. Febo, *Journal of Geophysical Research: Atmospheres*, 2000, **105**, 14585.
4. J. F. Stanton, B. A. Flowers, D. A. Matthews, A. F. Ware and G. B. Ellison, *J. Mol. Spectrosc.*, 2008, **251**, 384.
5. A. C. Vandaele, C. Hermans, P. C. Simon, M. Carleer, R. Colin, S. Fally, M. F. Merienne, A. Jenouvrier and B. Coquart, *J. Quant. Spectrosc. Radiat. Transfer*, 1998, **59**, 171.
6. J. Lelieveld, S. Gromov, A. Pozzer and D. Taraborrelli, *Atmos. Chem. Phys.*, 2016, **16**, 12477.
7. R. K. Talukdar, J. B. Burkholder, M. Hunter, M. K. Gilles, J. M. Roberts and A. R. Ravishankara, *J. Chem. Soc., Faraday Trans.*, 1997, **93**, 2797.
8. IUPAC, Task Group on Atmospheric Chemical Kinetic Data Evaluation, (Ammann, M., Cox, R.A., Crowley, J.N., Herrmann, H., Jenkin, M.E., McNeill, V.F., Mellouki, A., Rossi, M. J., Troe, J. and Wallington, T. J.). Last access Sept. 2023, https://iupac.aeris-data.fr/).
9. W. Tsang and R. F. Hampson, *J. Phys. Chem. Ref. Data*, 1986, **15**, 1087.
10. J. Burkholder, S. Sander, J. Abbatt, J. Barker, C. Cappa, J. Crounse, T. Dibble, R. Huie, C. Kolb and M. Kurylo, *Chemical kinetics and photochemical data for use in atmospheric studies; evaluation number 19*, Jet Propulsion Laboratory, National Aeronautics and Space Administration, 2020.
11. E. Assaf, C. Schoemaecker, L. Vereecken and C. Fittschen, *Phys. Chem. Chem. Phys.*, 2018, **20**, 10660.